2013-01-07

The Hydrological Impact of a Mountain Pine Beetle Infestation on the Upper Elbow River Watershed

Shawn, Tse

UNIVERSITY OF CALGARY

The Hydrological Impact of a Mountain Pine Beetle Infestation on the Upper Elbow River Watershed

by

Shawn Knor Tse

A THESIS

SUBMITTED TO THE FACULTY OF GRADUATE STUDIES

IN PARTIAL FULFILLMENT OF THE REQUIREMENTS FOR THE

DEGREE OF MASTER OF ENGINEERING

DEPARTMENT OF CIVIL ENGINEERING

CALGARY, ALBERTA

JANUARY, 2013

Abstract

To determine the hydrological impact of a large-scale mountain pine beetle (abbreviated as MPB) infestation on the Upper Elbow River watershed, a hydrological model was created and calibrated using a dataset from Alberta Environment over the years 2003 – 2005. The root mean squared error of the flow was approximately 10.48 m^3/s. The greatest error occurred in Jun 2005 where a much higher amount of precipitation than the previous two years was recorded. An MPB model was used to simulate an epidemic infestation. Various different scenarios were attempted, but the increase in the water yield of the Elbow River watershed could not be confirmed.

Acknowledgements

I would like to thank Dr. Caterina Valeo and Dr. Axel Anderson for giving me research and teaching opportunities in my studies.

My gratitude also goes to the University of Calgary and the NSERC program for providing research funding.

Thanks also go to Ghazi Al-Rawas for providing DEM data, and soil data, the Water Survey of Canada for the streamflow data, and Alberta Agriculture and Nishad Wijesekara for meteorological data. My research would not have been possible without any of these data sets.

I would also like to thank the support staff of CRHM, Dr. John Pomeroy, Tom Brown, and Kevin Shook for giving me a great deal of support and help in understanding their model.

Last but not least, I would like to thank my family and friends for all of the support they have given me throughout my thesis.

Table of Contents

List of Figures

List of Tables

1 Introduction

The mountain pine beetle (*Dendroctonus ponderosae*, abbreviated as MPB) is an insect native to North America that lives in the trunks of pine trees, eventually killing its host (Coggins, Coops, & Wulder, 2008). An outbreak in British Columbia started in 1999, destroyed 13 million hectares and 47% of all merchantable pine by mid-2008, and threatened to spread to Western Alberta. (BC Ministry of Forests and Range, 2012; Maclauchlan, 2009).

Alberta Environment and Sustainable Resource Development, which intends to minimize the spread of the infestation on the eastern slopes of the Rocky Mountains, would like to understand how an MPB infestation would affect the flow parameters of the Elbow River watershed, which provides drinking water for the City of Calgary.

The objective is to model the hydrology of the Upper Elbow River watershed using a lumped model approach. This model would be designed with the ability to simulate the impacts of a large MPB infestation on vegetation and its effects on flow rates in the Elbow River watershed.

The watershed must first be partitioned into sections sharing hydrological properties, and a MPB infestation will be simulated by reducing the effective LAI in the area. The water output will be compared between the pre-disturbed and post-disturbed models. Therefore the model must simulate the effect of canopy and evapotranspiration on hydrology.

2 Literature Review

The topography, climate, soil, and vegetation all interact in a variety of ways, producing a complex mix of states (e.g. soil characteristics, plant health) and processes (e.g. evaporation and transpiration). A significant amount of rain is caught by the forest canopy, in a process called interception. This captured water undergoes different processes than rainfall on open ground (Hélie, Peters, Tattrie, & Gibson, 2005; Pugh & Gordon, 2012; Strasser, Warscher, & Liston, 2011). The remaining rain reaches the ground, where it will either be absorbed by the vegetation, move into the groundwater table, or become surface water. Surface water quickly flows downhill, and successively aggregates to larger rivers until it finally reaches a lake or an ocean.

Sunlight hitting these waters will cause evaporation at any point during this flow. As can be seen, the major drivers of the hydrological cycle are solar radiation and gravity (Hélie *et al.*, 2005). Each important process will be outlined and discussed in detail below, followed by a discussion on the mountain pine beetle and its effects on the hydrological cycle. Finally, the study area will be briefly described.

2.1 Water Balance

The water balance equation is used to describe and correctly account for the flow of water in and out of a system and, in its simplest form, is:

$$P + I = Q + E + \Delta S \text{ , where} \tag{2.1}$$

P	Precipitation, as rain or snow
I	Inflow, for example upstream flow or from deep aquifers
Q	Outflow
E	Evaporation and transpiration
ΔS	Change in storage within the system

Using the water balance, water that spontaneously 'appears' or 'vanishes' in a model time step reveals mistakes in the mathematical model that can be found and corrected.

2.2 Precipitation, Interception, and Sublimation

Air temperature is the main factor in determining whether precipitation falls as rain or snow. If the air temperature is below freezing point, the precipitation falls as snow (US Army Corps of Engineers [USACE], 2000). The algorithm can be described as follows:

$$\begin{cases} P_{rain} = P, P_{snow} = 0 & T_a \geq PX_{temp} \\ P_{rain} = 0, P_{snow} = P & T_a < PX_{temp} \end{cases}, \text{where} \tag{2.2}$$

P_{rain}	Rainfall [mm]
P_{snow}	Snowfall [mm water equivalent]
T_a	Mean air temperature [degrees C]
PX_{temp}	Threshold air temperature [degrees C]

Forest canopies can intercept up to 60% of cumulative annual snowfall, resulting in a 30 - 40% annual loss of accumulated snow cover in boreal coniferous forests (Strasser *et al.*, 2011; Pugh & Gordon, 2012). From the intercepted snow, as much as 31 - 40% (19 - 24% of total snowfall) is sublimated to the atmosphere (Pugh & Gordon, 2012; Hedstrom & Pomeroy, 1998; Strasser *et al.*, 2011).

Snow interception increases with canopy density, amount of exposed surface (i.e. LAI, explained below), and decreases with density of falling snow, temperature, and wind speed (Strasser *et al.*, 2011; Hedstrom & Pomeroy, 1998; Pugh & Gordon, 2012). The interception capacity of pine trees was found to be 3 – 8 mm with only small differences between species (Jost, Moore, Smith, & Gluns, 2012; Schmidt & Gluns, 1991).

Leaf Area Index (LAI) is a unitless variable that describes the leafiness of the forest canopy. Often LAI', or effective LAI, is used because aerial photography can only capture LAI as leafy area including the woody branches (Pugh & Gordon, 2012). Larger LAI numbers mean that incoming radiation will strike more foliage on the way down, limiting the light that reaches the forest floor (Wigmosta, Vail, & Lettenmaier, 1994). LAI is calculated by taking the area of the upper surface of each leaf or needle, and dividing it by the area occupied by the tree.

Horizontal Canopy Coverage, or fractional crown closure, is the proportion of rain that is captured by the canopy. It is a number between 0 (no cover at all) and 1 (complete interception) that is described empirically with the equations below and used to determine the maximum amount of rain supported by the canopy:

$$Cc = 0.29 \log_{10}(LAI) + 0.55 \text{ , where} \tag{2.3}$$

$$S_{rainMax} = \min \begin{pmatrix} Cc \times LAI \times 0.2 \\ 0.04 \times S_{snow} \end{pmatrix} \text{, where} \tag{2.4}$$

Cc	Horizontal Canopy Coverage [unitless]
LAI	Leaf Area Index [unitless]
$S_{rainMax}$	Maximum amount of rain supported by the canopy [mm equiv.]

S_{snow} Water storage in the canopy in the form of snow [mm equiv.]

The maximum amount of snow supported by the canopy can be calculated using the density of fresh snow and LAI, from Hedstrom and Pomeroy (1998):

$$L^{*} = S \times LAI = \bar{S}(0.27 + 46.0/\rho_s) \times LAI \text{ , where} \quad (2.5)$$

L^{*} Maximum amount of snow supported by the canopy [mm equiv.]
S Maximum snow load per unit branch area [kg/m²]
$\bar{S}$ Species-specific maximum canopy snow interception load [kg/m²]
ρ_s Density of fresh snow [kg/m³]

The empirical parameter $\bar{S}$ is a species-specific average value ranging between 0 – 100 kg/m². Schmidt and Gluns (1991) suggest values of 6.6 kg/m² for pine trees, and 5.9 kg/m² for spruce trees. The density of fresh snow as a function of temperature was first developed by the US Army Corps of Engineers and adjusted by Schmidt and Gluns (1991):

$$\rho_s = 67.92 + 51.25e^{T/2.59} \text{ , where} \quad (2.6)$$

T Mean air temperature [degrees C]

If the snow storage limit is below the amount of intercepted snow currently held in the canopy, snow will slough off the canopy. Afterwards, falling snow adds to the snow's canopy storage, and if the snowfall is below a threshold, the snow storage is affected by wind speed.

2.3 Net Radiation

Net Radiation governs the processes of evapotranspiration and is the sum of two components – net shortwave radiation (K_n) and net longwave radiation (L_n). In many cases the units given for energy are in Watts per square meter [W/m²], or Megajoules per square meter per day [MJ/m²/day]. Both the shortwave and longwave radiation components will be elaborated below.

2.3.1 Shortwave Radiation

Incoming shortwave radiation, or solar radiation, is direct radiation from the sun. The amount of solar radiation received by the environment varies depending on the time of year, cloud cover, and albedo.

Net shortwave radiation is the solar radiation received minus the amount reflected back:

$$K_n = K_{\downarrow} - \alpha K_{\downarrow} = (1 - \alpha) K_{\downarrow} \text{ , where} \qquad (2.7)$$

α albedo
$K_{\downarrow}$ Incoming shortwave radiation

Incoming shortwave radiation is often measured by weather stations, but the Food and Agriculture Organization of the United Nations (1998) uses Hargreaves' radiation formula if the data is unavailable. The equation, a function of maximum and minimum temperature, was adjusted by Annandale, Jovanovic, Benadé and Allen (2002):

$$K_{\downarrow} = k_{K_{\downarrow}}(1 + 2.7 \times 10^{-5} Alt) \times \sqrt{T_{max} - T_{min}} R_a \text{ , where} \quad (2.8)$$

$k_{K_{\downarrow}}$	Adjustment coefficient for interior or coastal regions [degrees C$^{-0.5}$ / m]
Alt	Altitude above the earth's surface, linked to the weather station [m]
T_{max}	Maximum air temperature [degrees C]
T_{min}	Minimum air temperature [degrees C]
R_a	Potential extra-terrestrial solar radiation [W/m^2]

The adjustment coefficient is 0.16 degrees C$^{-0.5}$ / m for interior locations, where land mass dominates, and 0.19 degrees C$^{-0.5}$ / m for coastal regions where air masses are strongly influenced by adjacent water bodies. (Annandale *et al.*, 2002)

Latitude and DOY (day of the year, a value between 1 and 366, with Jan 1 being 1) are then used to calculate the potential extra-terrestrial solar radiation, that is, the Sun's radiation just before it enters the atmosphere (Annandale *et al.*, 2002) (American Society of Civil Engineers [ASCE], 2005):

$$\delta = 0.409 \sin\left(\frac{2\pi}{365} DOY - 1.39\right) \quad (2.9)$$

$$\omega_s = \operatorname{acos}(-\,tan(\phi)\,tan(\delta)) \quad (2.10)$$

$$D_{rel} = 1 + 0.0338 \cos\left(\frac{2\pi}{365} DOY\right) \quad (2.11)$$

$$R_a = \frac{G_{sc} D_{rel}}{\pi} [\omega_s \sin(\phi) \sin(\delta) + \sin(\omega_s) \cos(\phi) \cos(\delta)] \quad (2.12)$$

δ	Solar declination, the angle away from the celestial equator [radians]
DOY	Day of the year, an integer between 1 and 366
ω_s	Sunset hour angle [radians]
ϕ	Latitude [radians]
D_{rel}	Inverse relative distance factor, squared, between the earth and the sun [unitless]
G_{sc}	Solar constant (1367 W/m^2)

2.3.2 Longwave Radiation

Net longwave radiation can be approximated as a function of temperature range and vapour pressure with a formula provided by the ASCE (2005):

$$L_n = f_{cd}\epsilon_{atm}\sigma[(T_{max} + 273.15)^4 + (T_{min} + 273.15)^4\ ]/2 \text{ , where} \qquad (2.13)$$

f_{cd}	Cloudiness factor [unitless]
ϵ_{atm}	Clear sky net emissivity of the Earth's atmosphere [unitless]
σ	Stefan-Boltzmann constant (5.670400×10^{-8} W/m²/K⁴)
T_{max}	Maximum air temperature [degrees C]
T_{min}	Minimum air temperature [degrees C]

Clear sky net emissivity of the Earth's atmosphere is dependent on the temperature and humidity profile of the entire atmospheric column, but it can be estimated with actual vapour pressure from Annandale *et al.* (2002):

$$\epsilon_{atm} = \left(0.34 - 0.14\sqrt{e_a}\right) \text{ , where} \qquad (2.14)$$

e_a	Actual vapour pressure of the atmosphere [kPa]

The cloudiness function is normally used for daily and monthly time steps, but for a weekly time step it can also be used. It is an empirical linear function based off of the solar radiation and the clear sky radiation:

$$R_{so} = (0.75 + 2 \times e^{-5}Elev)R_a, \quad 0.3 \le R_{so} \le 1.0 \qquad (2.15)$$

$$f_{cd} = 1.35\frac{K_{\downarrow}}{R_{so}} - 0.35 \qquad (2.16)$$

R_{so}	Clear-sky solar radiation – amount of solar radiation that reaches the ground under clear-sky conditions [W/m²]
$Elev$	Elevation above mean sea level [m]
R_a	Potential extra-terrestrial solar radiation [W/m²]

The constant 0.75 represents the maximum clear sky transmissivity of the atmosphere.

The vapour pressure of the air can be found from relative humidity and air temperature readings by relating the following equations:

$$e_a = 6.11 \times 10^{7.5T_d/237.7+T_d}/10 \quad (2.17)$$

$$e_s = 6.11 \times 10^{7.5T/237.7+T}/10 \quad (2.18)$$

$$RH = e_a/e_s \times 100 \quad (2.19)$$

$$e_a = \frac{RH}{100} \times 6.11 \times 10^{7.5T/237.7+T}/10 \quad (2.20)$$

T_d	Dewpoint temperature [degrees C]
e_s	Saturated vapour pressure of the air [kPa]
T	Air temperature [degrees C]
RH	Relative humidity (between 0 and 100)

From these equations, it is clear that saturated vapour pressure is a function of temperature. The slope of this function, known as Δ, will be important in determining the amount of evaporation in the following section.

2.4 Evaporation and Transpiration

Evapotranspiration (ET) varies by tree species, and is significantly affected by the length of the growing season. After snowmelt, transpiring forests draw water from the soil, and when the trees senesce and die, they take up less water through their root systems, reducing ET (Pugh & Gordon, 2012). When evaporation dries the soil surface, water from deep down in the soil will rise through capillary action and moisturize the surface. This wicking process will continue until there is no longer any moisture in the soil (Wigmosta *et al.*, 1994). Water not lost to evaporation or transpiration eventually becomes a part of the streamflow or groundwater system (Hélie *et al.*, 2005).

In 1972, Priestley and Taylor proposed a formula to estimate evaporation on advection-free surfaces. When a surface has a large enough area, lateral energy transfer from adjacent dry areas is negligible, and it can be considered advection-free (Hayashi, 2011). The Priestley-Taylor formula is:

$$E_{pe} = \alpha_e \frac{\Delta}{\Delta+\gamma} Q_{ne} \text{ , where} \qquad (2.21)$$

E_{pe}	Amount of evaporation from a wet surface
α_e	Empirically-based coefficient [unitless]
Δ	Slope of the saturated vapour pressure-temperature curve [kPa/degrees C]
γ	Psychometric constant [kPa/degrees C]
Q_{ne}	Available energy for evaporation

The slope of the saturation vapour pressure-air temperature curve is a function of air temperature, T [degrees C] and is calculated as such (ASCE, 2005):

$$\Delta = \frac{2503 \exp\left(\frac{17.27T}{237.3+T}\right)}{(T+237.3)^2} \qquad (2.22)$$

The psychometric constant is an estimation of the partial pressure of water vapour in air. Being a function of air pressure, the following equation can be used:

$$\gamma = 0.000665P, \text{ where } P \text{ is atmospheric pressure [kPa]} \qquad (2.23)$$

Sumner and Jacobs (2005) developed an empirical formula to calculate α_e based from LAI and solar radiation:

$$\alpha_e = \left(aK_{\downarrow} + bK_{\downarrow}^2 + c\right)(d \times LAI + 1), \text{ where} \qquad (2.24)$$

a empirical coefficient (-9.95×10^{-4} m^2/W)
b empirical coefficient (6.36×10^{-7} m^4/W^2)
c empirical coefficient (0.801)
d empirical LAI factor (0.657)

R_n is used for Q_{ne} , and uses the difference between shortwave radiation (K_n Equation (2.7) and Hargreaves' formula, Equation (2.8)) and net longwave radiation (Equation (2.13)). These both require R_a, potential extra-terrestrial solar radiation, which use Equations (2.9 – 2.20) to calculate.

If the ground and understory are covered with a layer of snow, then they will not contribute to evapotranspiration (Gray & Landine, 1987).

2.5 Snowpack, Snowmelt and Surface Water

Snowmelt can be modelled with a basic temperature index solution:

$$M = c(T_a - T_b) \text{ , where} \qquad (2.25)$$

M Snowmelt [mm / time step]
c Melt rate coefficient [mm / time step / degree C]

T_a	Air temperature [degrees C]
T_b	Fixed base temperature [degrees C]

Assuming a daily melt computation interval, the melt rate coefficient would usually be between 0.282 - 0.564 mm/°C/day when used with a recorded maximum temperature, and 0.564 - 1.411 mm/°C/day when used with average air temperature (USACE, 1994). The choice of base temperature depends on computation interval and form of temperature data, but it is normally around freezing point.

Another temperature index method can be described based on experiments done by Pellicciotti *et al* (2005), which takes into account both temperature and incoming shortwave radiation (Empirical E Equation):

$$melt = TF \times T + SRF \times (1 - \alpha_{snow})K_{\downarrow} \text{ , where} \qquad (2.26)$$

$melt$	Amount of snowmelt [SWE mm / week]
TF	Temperature Factor (8.4 mm / degrees C)
T	Air Temperature [degrees C]
SRF	Shortwave Radiation Factor (1.5792 mm / (W/m^2))
α_{snow}	Albedo of snow [unitless]
$K_{\downarrow}$	Incoming shortwave radiation [W/m^2]

The temperature and shortwave radiation factors are derived empirically. The albedo of fresh snow (0.85) is used each time more than 3 cm of snow falls (Winkler *et al.*, 2010); otherwise for each time step, the albedo decays by 0.042 if there are no conditions for melt, or by 0.497 in melt conditions. The albedo affects the amount of incoming shortwave radiation absorbed by the snow and therefore the amount of melt.

The maximum storage capacity of liquid water in the snowpack is calculated from observations by Denoth (2003) who found that the snowpack could reach a saturation of about 4% per volume before gravity would start to draw liquid water out of it:

$$S_{wi} = 4\% \times snow_{depth} \times \varphi_{snow} = 0.04 \times \frac{SWE}{\rho_s} \times \left(1 - \frac{\rho_s}{\rho_{ice}}\right) \text{, where} \qquad (2.27)$$

S_{wi}	Maximum storage capacity of liquid water [mm]
$snow_{depth}$	Depth of snow [mm]
φ	Porosity [mm / time step]
SWE	Snow (Water Equivalent) [mm]
ρ_s	Density of snow [kg/m3]
ρ_{ice}	Density of ice (916.7 kg/m3)

Meltwater or other water pushed out of the snowpack will either infiltrate into the soil or join the streamwater regime and flow downhill.

2.6 Infiltration and Percolation

Water infiltration into soil is governed by capillary attraction, gravity, and pressure. Soil moisture can be modelled as a reservoir with a sieve at the top. For a dry surface, the infiltration rate is equal to the rainfall rate up to a maximum infiltration rate. When this rate is exceeded, excess water immediately becomes runoff.

Soil moisture storage also has a maximum called infiltration capacity, f_m, or field capacity. When infiltration capacity is reached, water pools on the surface (Chang, 2003; Wigmosta *et al.*, 1994). Over time, the soil can recover its moisture capacity, losing its water to percolation, subsurface soil runoff, and evapotranspiration. This recovery rate withdraws a constant amount of moisture from the soil each time step until the soil is dry. The entire system is summarized as follows:

$$pe_t = \begin{cases} LWASS - f_c & LWASS > f_c, f_c \leq (S_{soilMax} - S_{soil}) \\ S_{soil} + LWASS - S_{soilMax} & LWASS > (S_{soilMax} - S_{soil}) \\ 0 & LWASS \leq (S_{soilMax} - S_{soil}) \end{cases} \text{, where} \tag{2.28}$$

pe_t	Runoff from soil moisture excess [mm]
$LWASS$	Liquid water at soil surface [mm]
f_c	Ultimate infiltration capacity of the soil [mm / time step]
$S_{soilMax}$	Maximum soil moisture storage [mm water equiv.]
S_{soil}	Current soil moisture storage [mm water equiv.]

Percolation is the movement of water downwards out of the soil layer and into the groundwater layer. In some models, the control surface does not extend to the groundwater and therefore percolation is considered to have left the system.

The water in the soil freezes in winter and forms a waterproof barrier, locking in soil moisture and preventing water from evaporating or percolating. This greatly restricts water movement until it is released during spring thaw, where it often becomes runoff and contributes to streamflow.

2.7 Runoff

In a weekly time step, runoff travels downhill to the largest river. For much smaller time steps, the hydrograph of the water, which is a depiction of the flow of the water over time, is routed and shaped by forces such as the surface roughness and hydraulic radius, but these factors do not come into play for larger time steps, particularly for steep rivers such as the Elbow River.

2.8 The Host-Pest Relationship

Dendroctonus ponderosae Hopkins is a bark beetle native to Western North America. About half a centimeter in length as an adult (Thomson & Shrimpton, 1984), it spends most of its life under the bark of a pine tree except for a few days when it flies out to find a new host. Its only food source is the phloem of the pine tree, which the tree uses to carry essential nutrients around (Silva Ecosystem Consultants Ltd. [Silva], 1993).

The MPB is a natural and integral part of the ecosystem within which it resides, and has been for centuries (Silva, 1993). Mountain pine beetles prefer pines in particular (Ritchie, 2008), among which are the lodgepole pine (*Pinus contorta*), the ponderosa pine (*Pinus ponderosae*), sugar pine (*Pinus lambertiana*), and white pine (*Pinus strobus*) (Safranyik, Barclay, Thomson, & Riel, 1999). Aging trees and mature stands are most susceptible to MPB attacks.

For the first 8 months after attack the tree will show few symptoms of being affected, but after the first year, the tree will die and the moisture content in its upper foliage gradually diminishes (Ritchie, 2008; Hélie *et al.*, 2005; Coggins, Coops, Wulder, Bater, & Ortlepp, 2010; Pugh & Gordon, 2012). This phase is called the green attack phase.

In the red attack phase, dead pine trees will eventually develop discoloured needles as moisture leaves them. In this 2 to 4 year period after infestation (Ritchie, 2008; Pugh &

Gordon, 2012), the needles will fade in colour to yellowish green to red, and finally brown (Skakun, Wulder, Franklin, 2003; Winkler, Boon, Zimonick, & Baleshta, 2010).

Fading begins at the base of the tree and gradually moves upwards. At the gray attack stage 3 years after the attack, the tree will have lost its needles and small branches will begin to fall off (Coggins *et al.*, 2010). A couple years later, all the foliage will be lost and the tree's susceptibility to fire will be a large concern. Eventually the entire tree will fall over and become a part of the understory, which occurs 4 – 15 years after infestation (Pugh & Gordon, 2012).

When beetles emerge to infect new trees, they will usually disperse less than 30 m from the host tree (Safranyik, Linton, Silversides, & McMullen, 1992). Up to 0.2% of beetles disperse from the stand and travel on warm air thermals hundreds of metres, sometimes hundreds of kilometres to infest new stands (Safranyik *et al.*, 1992). It is suspected that new infestations from distant locations are from beetles travelling above the canopy (Safranyik *et al.*, 1992).

The spread of a locally produced beetle population into surrounding trees and adjacent stands is somewhat predictable. However, the flight of MPB and their long-range dispersal is much more difficult to predict.

2.8.1 Hydrological Impacts of Epidemic Infestation

Experts agree that a large-scale and destructive infestation will change water parameters. Streamflow in devastated stands is expected to be greater in magnitude, respond to storm events more quickly, and have a greater number of peak flow events. As trees are infected, die, and are felled, their absence will have a number of impacts on the local hydrological cycle, resulting in increased annual water yields (Potts, 1984), and larger and earlier peak flows in rivers (Winkler, 2009; Schnorbus, 2009).

Needle loss of killed trees only marginally affects summer albedo, but O'Halloran *et al.* (2011) found that in BC and Oregon, winter albedo of coniferous forests increased by 0.06 at 4 years following attack, due to exposure of the snow at ground surface.

A number of studies done appear to confirm these results for British Columbia (Schnorbus, 2009; Hélie *et al.*, 2005; Canadian Forestry Service, 1982; Potts, 1984); however, Bosch and Hewlett revealed in their review of paired watershed experiments that the annual precipitation must exceed 450 mm in order to detect an increase in runoff as a result of removing substantial amounts of vegetation cover in a watershed (Hélie *et al.*, 2005). One study used girdling as an analogue for a beetle attack, causing 60% tree mortality increasing modelled water outflow by 92% (Pugh & Gordon, 2012).

A report made by the Canadian Forestry Service (1982) estimated that water yields would increase from 16-20% in forested areas with total kill and trees left standing, with estimates climbing as high as 34%, depending on the cutting pattern and the extent of forest cover. It predicted that most of the increased runoff would occur during the snowmelt period, and that salvage logging would accentuate these changes.

2.8.2 Modelling

Sims, Aadland, and Finnoff (2010) developed a model to calculate the growth and spread of MPB, which models the infestations in a predator-prey fashion, adjusting the LAI based on the proportion of remaining un-killed trees:

$$B_n = \phi(\pi_{n-1}A_{n-1})^{\nu} \text{ , where} \tag{2.29}$$

B_n	Beetles per acre at time-step n
ϕ	Fecundity – average beetle offspring per infested tree
π_n	Pest Mortality – proportion of adult trees killed at time-step n
A_n	Susceptible adult trees at time-step n
ν	Curvature parameter – rate of decrease in beetle reproduction with increases in beetle-induced mortality in adult trees

The beetle population is then used to determine the pest mortality:

$$\pi_n = \frac{B_n^2}{B_n^2+a^2} \text{ , where} \tag{2.30}$$

a	Beetles per acre needed for a 50% chance mortality in adult trees. The default value in Sims et al. (2010) is 250,000

Then the tree population is separated based on age and counted out:

$$X_n = (1-\delta_X)X + b_Y Y + b_A A \tag{2.31}$$

$$Y_n = (1 - \delta_Y)Y + \delta_X X \tag{2.32}$$

$$A_n = (1 - d - \pi_n)A + \delta_Y Y - h_{tA} \tag{2.33}$$

X_n	Seeds at time-step n
Y_n	Young trees at time-step n
δ_X	Proportion of seeds that grow to young trees
δ_Y	Proportion of young trees that mature to susceptible adults
b_Y	Seeds planted by young trees (as a proportion of young trees)
b_A	Seeds planted by adult trees (as a proportion of adult trees)
d	Proportion of trees killed naturally
h_{tA}	Trees harvested commercially

The resulting effective LAI is calculated and used as an indicator of forest stand health:

$$LAI_{eff} = LAI \frac{A_n + Y_n}{A_{n-1} + Y_{n-1}} \tag{2.34}$$

2.9 Elbow River Watershed

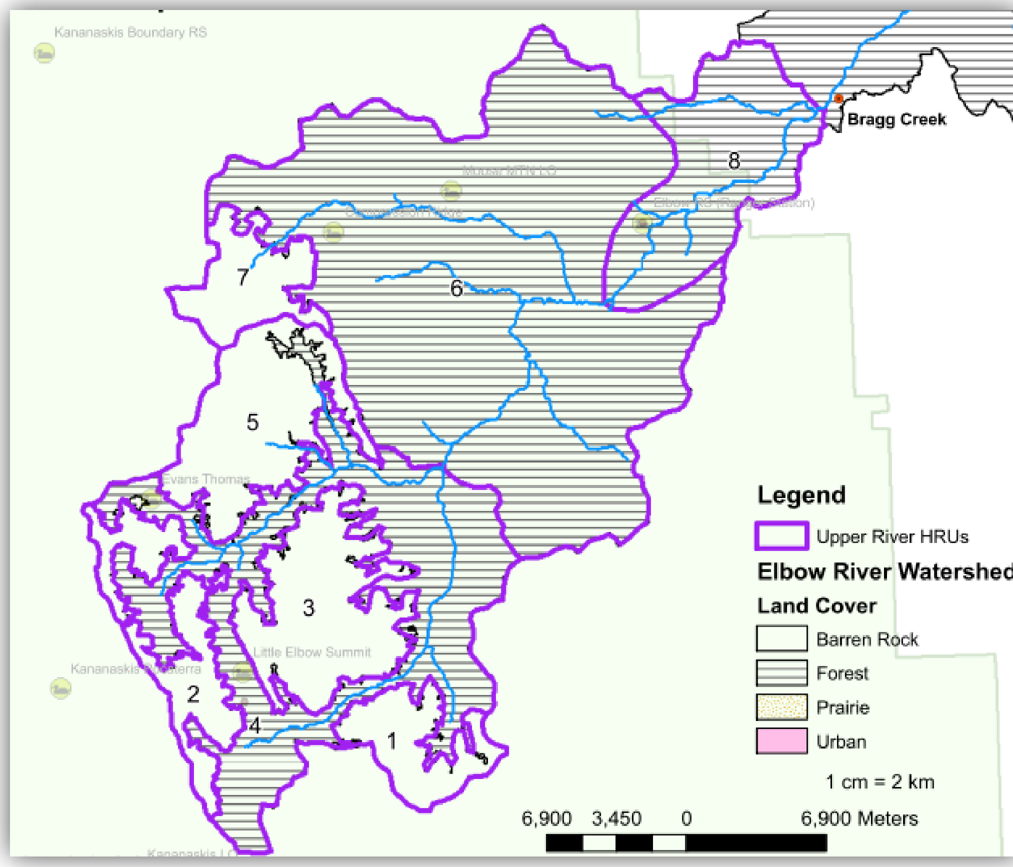

Figure 1: The Elbow River watershed

The Elbow River watershed is situated in the Canadian province of Alberta, bounded by the latitudes of 51°07" and 50°37" N and the longitudes of 115°06" and 114°00" W. In UTM coordinates, the region is situated in Zone 11N, between the northings of 5609400 and 5668000 m, and the eastings of 622975 and 711150 m. UTM is based on the WGS 84 ellipsoid.

The headwaters of the Elbow River start just outside of the Peter Lougheed Provincial Park, approximately 70 kilometres southwest of Calgary in the Opal and Misty Ranges.

The Bragg, Canyon, Lott, and Quirk creeks all contribute to the Elbow River before it reaches Calgary. The river runs through the urban areas of Bragg Creek, Redwood Meadows, and Calgary. Near the Calgary city limit, the Elbow River enters the Glenmore Reservoir, and it finally ends at the Bow River 2 kilometres downstream.

The Elbow River watershed feeds the Glenmore Reservoir, which is a storage reservoir for Calgary and is used for recreation and drinking water. The dam is used for flood management. Approximately 40% of Calgary's drinking water comes from the Elbow River (Bow River Basin Council, 2005).

The total drainage basin of the watershed is 1,235 km^2, and its length is approximately 119 km. The study area covers approximately 785.81 km^2 of this drainage basin, which is about 63.6% or 108 km of the river's reach, and the area's elevation ranges from 990 to 3139 m above mean sea level. The flow of the Elbow River peaks in early June and reaches its lowest levels in the winter, when the water is stored in the snowpack.

The climate of the region is classified by the Koppen climate classification system as Dfc, with Dfb in the urban areas and ET in the eastern frontal range of the Rocky Mountains. (Longley, 1972). From late October to late March, the temperature is normally below freezing, but chinook winds in the midst of winter cause the lower foothills to warm and cool rapidly. This fluctuation in temperature causes a series of melt periods during winter, removing the snow cover well before the onset of spring. The continental air masses moving through the region produce maximum temperatures in the range of 32 –

40 degrees C. The air masses move quickly in the spring and fall, creating rapid changes in conditions (Dai, 2010).

The region has a fairly steep slope to its outflow in the Bow River, so impacts in the river's upper reach quickly travel downstream without being greatly affected or muted. Precipitation tends to be the greatest in the mountainous areas in this region, due to orographic effects. Rainfall from May 1 to August 31 varies from slightly below 200 mm in the driest prairie areas to more than 325 mm in the mountains. From September 1 to April 30, precipitation varies from less than 150 mm in the driest prairie region to more than 275 mm in the mountains (Dai, 2010).

2.10 Thesis Objectives

The main objective in this thesis is to create a model to simulate the hydrological balance in the Elbow River watershed for the purposes of modelling a widespread MPB infestation. There have not been many empirical studies conducted on the influence of an MPB epidemic on a watershed (Pugh & Gordon, 2012). Therefore, it is important to create a model which can be used for these types of studies.

3 Research Methodology

In order to study the impact of an MPB infestation, a forestry hydrological model was programmed in MATLAB. Appropriate climate data, vegetation and soil data for the study region of the Upper Elbow River watershed was gathered and used to create a set of Hydrological Response Units (HRUs) for the study area. Water flow data from Bragg Creek station was then used to calibrate the model.

3.1 Methodology

Initially, existing hydrology models were examined to determine their suitability for modelling the characteristics of the Upper Elbow River watershed. Because the MPB can take a year to kill a pine tree, observable effects on foliage may not appear for many days. Therefore a weekly time step was chosen for the model. After experimenting with various models, MATLAB was used to program a lumped hydrological model.

The Elbow River watershed was divided into various HRUs, each with a characteristic soil type, land cover, or drainage pattern. Daily climate data acquired such as wind speed, air temperature, and relative humidity were spatially interpolated using a 2D smoothing thin-plate spline algorithm for temperature, snowpack, and precipitation readings, and a mean for wind readings and relative humidity. Once the model was coded, it was calibrated with existing flow data from Bragg Creek.

3.1.1 Historical Climate Data from Alberta Agriculture

Alberta Agriculture applied interpolation algorithms on various meteorological stations across Southern Alberta, producing climate data for every township in Alberta from 1961 – 2005. The climate parameters calculated included average daily air temperature, minimum and maximum daily air temperature, soil moisture in the top 120 cm, snowpack height [mm], potential and actual ET [mm equiv.].

3.1.2 Hydrometric Data

Water flow data from the Water Survey of Canada established a baseline of comparison to properly calibrate the model. Daily flow data was available for the Bragg Creek station, at coordinates 50°56'56" N and 114°34'15" W, station ID 05BJ004. The data ranged from 1934 to 2011, which extended beyond the study period of 2003 to 2005.

3.1.3 Vegetation Data – AVI – Alberta Vegetation Inventory

Alberta Environment and Sustainable Resource Development maintains a Vegetation Inventory which includes information such as crown closure and tree species. The data was collected mainly through airphoto interpretation and some field verification.

3.1.4 Soil Data

CANSIS – the Canadian Soil Information Service – divides their soil data into eight texture types: Very Coarse (VC), Coarse (C), Moderately Coarse (MC), Medium (M), Moderately Fine (MF), Fine (F), and bare rock, corresponding to PMTEX1,2 and 3 codes. These values were converted using the 38 texture classes of the USDA texture subclasses, using Table 5-8 of the Yukon Soil Database Manual (Gartner Lee Ltd, 2008), and a soil landscapes report from Agriculture Canada (Shields, Tarnocai, Valentine, & MacDonald, 1991), which translated these groups into the official USDA texture classes. Three soil types were found in the Upper Elbow River Watershed, Barren Rock, Fine and Moderately Fine areas and these were converted to Barren Rock, Clayloam, and Clay areas, respectively.

3.1.5 Elevation Data

A seamless digital elevation model (DEM) for NTS grid 82 J 11 NE in Southwestern Alberta was produced from Alberta Environmental Protection 1:20000 mapping data, and covers one mapsheet area with a minimum of 200 m overlap. Elevations were derived from a 100 m spaced grid, supported by irregularly-spaced sampling points, creating an interpolated 25 x 25 m DEM. The radiometric resolution of the data is 16 bits (256 unique values). The elevation ranges between 990 and 3139 m above sea level in the data.

3.2 Derivation of Hydrological Response Units

In order to determine the appropriate hydrological response units (HRUs) for the model, the 25 m DEM was first loaded into a GIS. Water flow and water accumulation maps were created to predict the locations of rivers and streams. From the river and stream map, a watershed catchment map was generated, simulating the drainage basins for the entire Elbow River watershed.

These sub-catchments were then separated based on land-cover: rocky terrain with no vegetation has hydrologic characteristics distinct from forested terrain with loamy soil. Forest borders were therefore used to separate the HRUs, and soil type was used to make a further division downstream in the foothills area. The final study region consisted of 8 HRUs: 5 rocky terrain HRUs and 3 forested HRUs, as shown in Table 1.

Table 1: Hydrological Response Units Chosen for the Upper Elbow Watershed

#	HRU Name	Vegetation	Area [km^2]	Area Percentage	Elevation Range [m]
1	Cougar Headwaters	Bare	26.77	3.407	1839 – 2927
2	Opal Range	Bare	38.15	4.855	1919 – 3050
3	Glasgow Range	Bare	59.27	7.543	1837 – 2980
4	Upper Basin	Forested	149.58	19.034	1601 – 3031
5	South Fisher	Bare	60.06	7.643	1714 – 3044
6	Loam Section	Forested	348.36	44.331	1401 – 2575
7	Canyon Creek Headwaters	Bare	28.17	3.585	1821 – 2744
8	ClayLoam Section	Forested	75.45	9.602	1299 – 1672
	UPPER ELBOW		**785.81**	**100.000**	**1919 – 3050**

The HRUs form the basis of the model, as water stored in these units is treated as a single reservoir with uniform properties within a hydrological unit. The GIS was also used to calculate the areas, elevation range, and geographic coordinates of each HRU. The final HRU map is shown in Figure 2, along with the river for comparison.

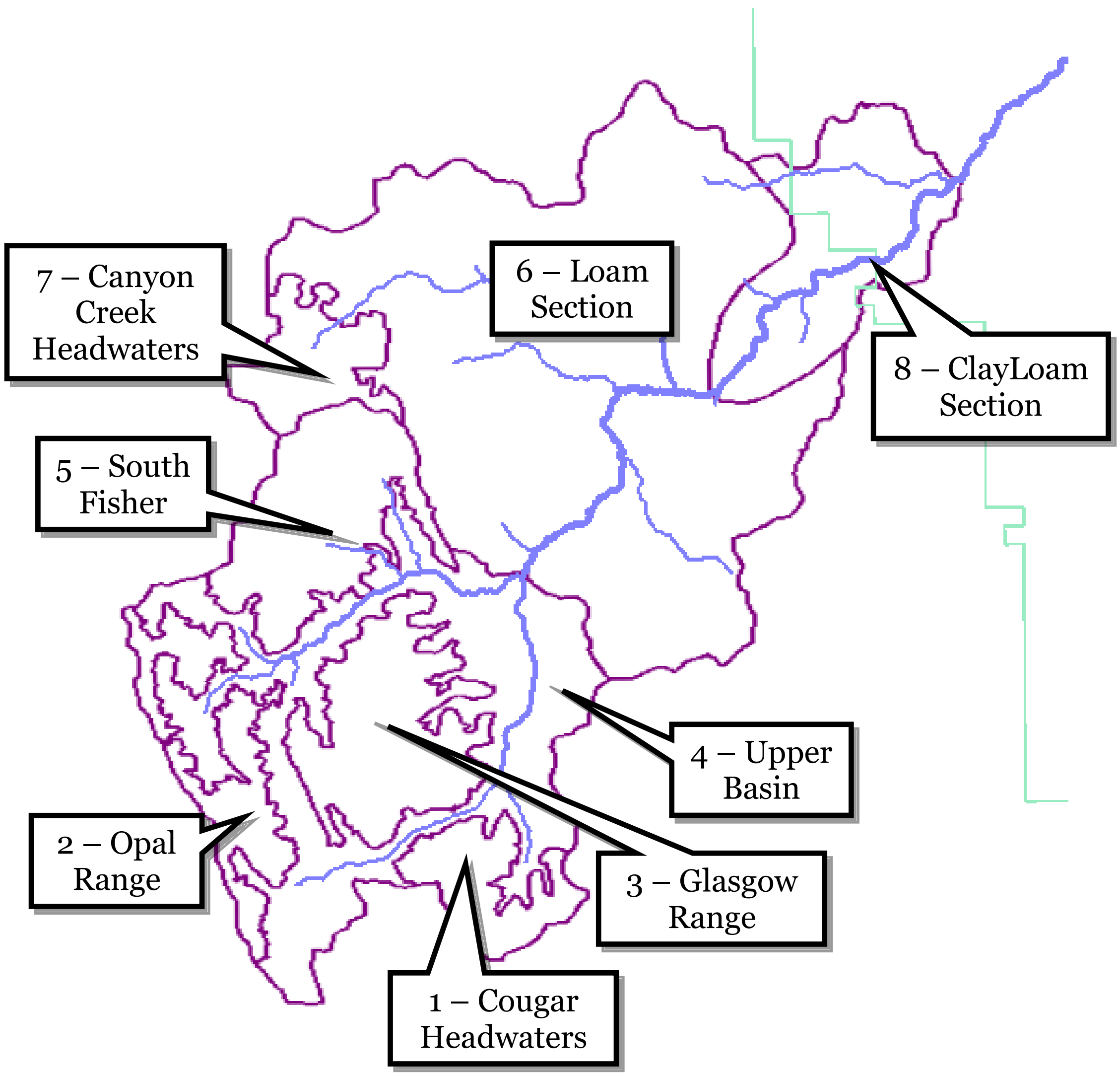

Figure 2: The final resulting HRUs, with names and ID numbers.

3.3 Model Structure

The model is programmed in MATLAB, with a basic object-oriented framework which contains the main features of the model: time-step-based model progression, calibration of individual parameters, and visualization of the behaviour of the model. The study period of the model was chosen to be 2003 – 2005 as this period had a good combination of dry years (2003) and wet years (2005), based on the water yield for those years. The workflow of the model is illustrated in Figure 3, below.

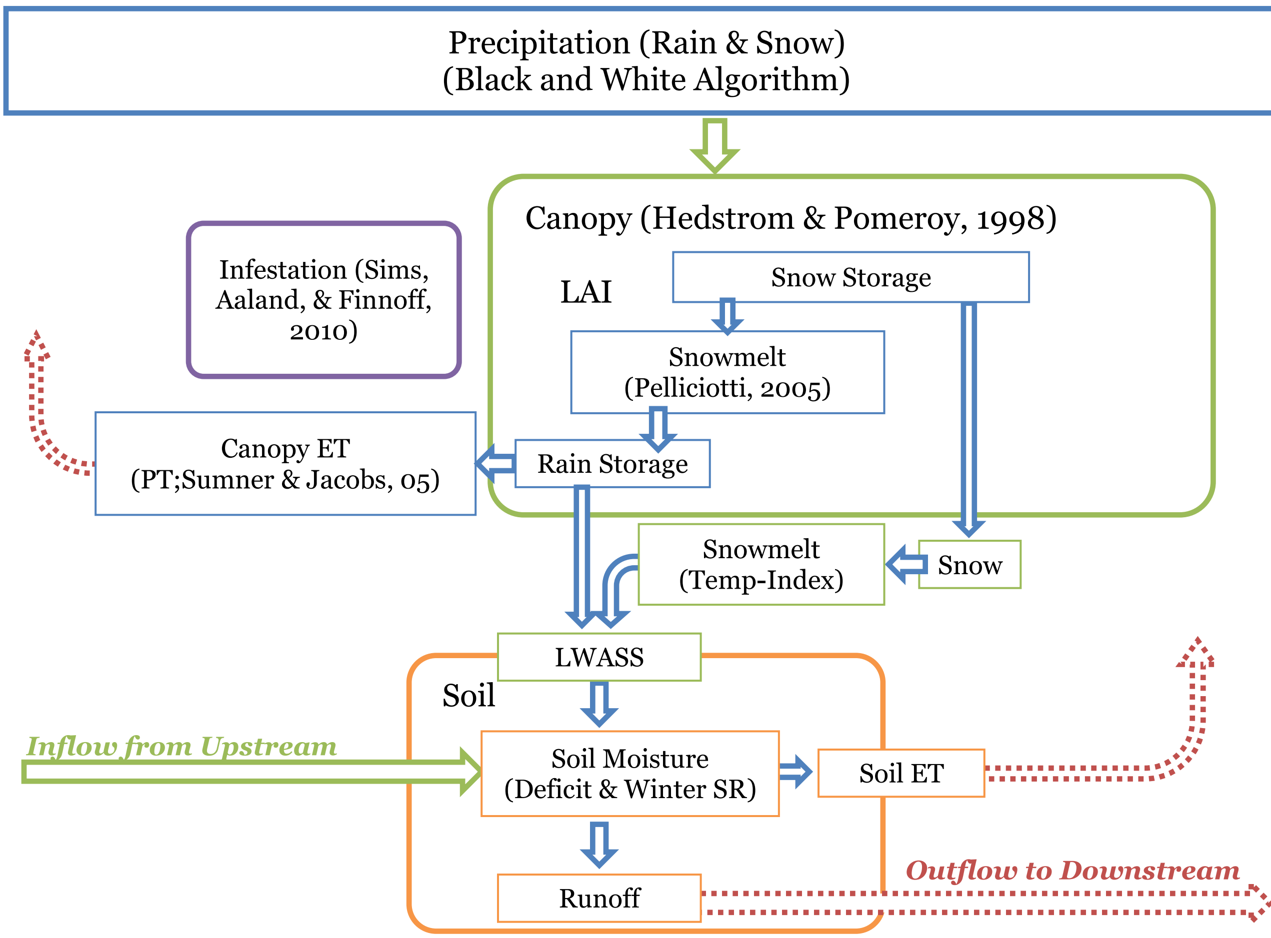

Figure 3: Workflow of the model

3.3.1 Aggregation of data

The climatological observations were read from files pre-generated on a township-by-township basis by Alberta Agriculture. The observations were aggregated to arrive at a single temperature or rainfall value for each HRU. The data was available as daily data which was aggregated to a weekly time step using the following methods in Table 2.

Table 2: Aggregation algorithms for observations

Observation	Model Name	Units	Aggregation Algorithm
Maximum Temperature	tmpMax	°C	maximum
Minimum Temperature	tmpMin	°C	minimum
Ave. Air Temperature	temp	°C	mean
Precipitation	ppt	mm	sum
Snow Depth	snodepth	mm	mean
Wind Speed	wind	m/s	mean
Relative Humidity	rh	%	mean
Soil Moisture	soil_moist	mm	mean
Stream Flow	flow	m^3/s	mean

Once all the data was converted to a weekly time step, it was then written to a set of files to optimize program execution.

3.3.2 Model Algorithms and Equation Flow

The model is organized as a series of algorithms, termed Modules, which interact with each other by interchanging variables. Each module represents a different hydrological process; this allows the different modules to be interchanged and for various proposed algorithms to be tested and evaluated. The program organizes the HRUs, termed HydroLumps, according to stream flow order, as seen in Figure 4.

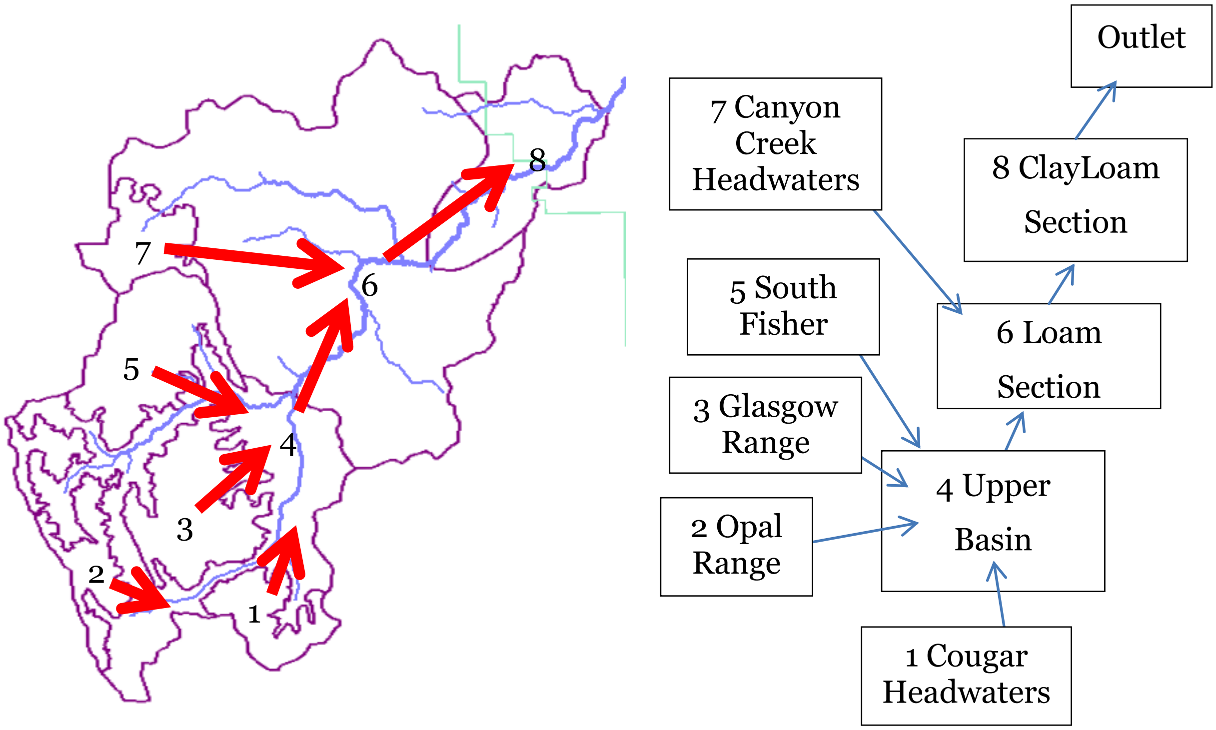

Figure 4: Stream Flow between HydroLumps

The hydrological flow within each HydroLump is calculated in the following order:

1. Inflow from an upstream HydroLump is added to this HydroLump
2. Precipitation module algorithm is run
3. Canopy module algorithm is run
4. Snow that falls through the canopy is added to the snowpack
5. Snowmelt module algorithm is run
6. Soil module algorithm is run
7. Soil runoff and upstream flow are combined to direct runoff
8. Outflow to downstream HydroLump is calculated

Each HydroLump uses a different module suitable for its specific characteristics, as specified in Table 3.

Table 3: Modules Chosen for each HydroLump

#	HydroLump Name	Canopy Module	Soil Module	Snow Module
1	Cougar Headwaters	NoCanopy	Impermeable	Snow
2	Opal Range	NoCanopy	Impermeable	Snow
3	Glasgow Range	NoCanopy	Impermeable	Snow
4	Upper Basin	PhysicalCanopy	DeficitNWinterSR	Snow
5	South Fisher	NoCanopy	Impermeable	Snow
6	Loam Section	PhysicalCanopy	DeficitNWinterSR	Snow
7	Canyon Creek	NoCanopy	Impermeable	Snow
8	ClayLoam Section	PhysicalCanopy	DeficitNWinterSR	Snow

The precipitation module used for all HydroLumps was the Black&White module. Evaporation was calculated as a submodule within the soil or canopy modules. For the DeficitNWinterSR module, a monthlyETWinter module was used, and for the PhysicalCanopy module, a special ETCanopy module was used to calculate evaporation.

Some modules are dependent on a flag that indicates whether or not it is winter at that particular time step. A different algorithm will run in winter than in the absence of winter. For this model, the winter flag is set when the snowpack is greater than 5 mm SWE or the average temperature is below zero. Each of the module algorithms will be explained in detail in the following sections.

3.3.2.1 Black&White Module

The Black&White module follows equation (2.2), which depends upon air temperature and the PX_{temp} parameter to determine if precipitation falls as rain or snow.

3.3.2.2 Canopy Modules

There are two canopy modules used in this model, NoCanopy and PhysicalCanopy. In NoCanopy, all rain and all snow falls to the ground. The snow adds to the snowpack, and the rain adds to the LWASS, which stands for Liquid Water at Soil Surface. Evaporation does not come into play for this module.

A more involved algorithm is used in PhysicalCanopy, with horizontal canopy coverage determined empirically. Effective LAI is a key parameter in the canopy model, and this is chosen in order to simulate the hydrologic effect of a beetle infestation, which would change this effective LAI parameter. Hedstrom and Pomeroy's (1998) formulas for determining snow and rain interception from LAI, and Sumner's equation, which provided a Priestley-Taylor coefficient for evapotranspiration create a model which uses LAI as a key parameter. Pine trees have an LAI of 2.2 (Hedstrom & Pomeroy, 1998; Winkler *et al.*, 2010)

Snowmelt is calculated from the Pellicciotti empirical E model in Equation (2.26), and added to the canopy rain storage, as the water can be held inside the snow. The liquid canopy interception is calculated with Equation (2.4).

After this point, the canopy undergoes evaporation, as calculated in the ETCanopy module, which uses Sumner's method (Equation (2.24)), an adjustment of the Priestley-Taylor equation, with an empirical multiplier to create an mm-equivalent number used in reducing the canopy storage. If all the intercepted water in the canopy has been dried up, the extra evapotranspiration energy will be used to dry the soil. If it is winter, however, no evapotranspiration occurs.

3.3.2.3 Snow Module

The Snow module uses the temperature-index equation (Equation (2.25)) to determine the amount of snowmelt per time step. The base temperature is 0 degrees C, and the melt rate coefficient *c* is calibrated separately for each HydroLump.

3.3.2.4 Soil Modules

Two soil modules are used in this model: Impermeable and DeficitNWinterSR. In the Impermeable module, the earth is treated as a rocky surface with no storage. Consequently, all inflow to this surface contributes to downstream runoff immediately. Evaporation is not considered for this module.

The HEC-HMS model (US Army Corps of Engineers, 2000) provides the theoretical basis for the DeficitNWinter model. Initially, the HEC-HMS program modelled soil moisture and infiltration with the Initial and Constant-Rate Algorithm, which had an initial loss, I_a, representing soil moisture deficit and depression storage. Depression storage is based on watershed topology, and as precipitation accumulates, it fills this initial loss value. Any excess precipitation would become runoff. In addition, if precipitation exceeded the ultimate infiltration rate f_c, then precipitation exceeding the infiltration would also run off, even if there was a moisture deficit in the soil. This model was adjusted to become quasi-continuous by adding a *recovery rate*, which was a fixed rate at which moisture would leave the soil after a prolonged period of no rainfall. The recovery rate was an abstraction of the combined evaporation rate and percolation rate.

The DeficitNWinterSR module modifies the quasi-continuous model, which uses Equation (2.28). Additional features were coded into this model to represent a winter ice lens, soil evaporation and soil runoff. The ultimate infiltrate rate was first estimated based on the soil category derived from CANSIS data, and then adjusted in the calibration stage for each HydroLump. During winter, soil moisture at the surface freezes and forms a lens, preventing water from infiltrating. Subsequently, infiltration is zero and all liquid water becomes runoff. Percolation is considered to be zero in wintertime as well. Some of the soil's moisture also leaks into the stream regime as soil runoff, this parameter is calibrated for each HydroLump.

The soil moisture is then subject to evaporation, either as spillover evaporation from the Canopy modules, or as a monthly constant based on recorded evaporation from Alberta Agriculture data.

3.3.2.5 Pest Module

The Pest module contains the algorithm for calculating the spread of the MPB infestation within an HRU, and it uses the algorithm developed by Sims *et al.* (2010) using Equations 2.29 – 2.34, referred to above. The key parameters for this module are beetle fecundity (ϕ), initial pest mortality (π_0), and curvature (ν).

3.3.2.6 Water Balance

At the end of each time step, the water balance (Equation (2.1)) for each HydroLump is calculated to ensure that no water is unexpectedly leaving or entering the system.

3.4 Potential Sources of Error

The current model does not include the uptake of water into the forest's vascular system, where it acts as water storage and can be released to the atmosphere as ET. Although the PhysicalCanopy algorithm has a transpiration component, in the current implementation, intercepted water must first be fully depleted before the soil will lose moisture. This results in an over estimation of runoff, as the soil moisture is not reduced as much as it should be. In addition, grey-attack stands may not be modeled properly, because canopy cover, such as trunks, branches and snags, are mostly vertically-oriented, and most interception models are designed for the randomly-oriented foliage of healthy stands (Bewley, 2010). Consequently, these interception models can overestimate intercepted water for grey attack stands, resulting in less synchronized snowmelt and flow.

The aggregation of the study area into HRUs may create errors due to the great range of elevations and aspects encountered. This makes it difficult to calculate a single incoming radiation value that is appropriate for all values of the watershed, causing snowmelt to be more synchronized and overestimating peak flow values. In addition, the mountains can occlude large sections of forest and thus reduce the amount of available sunlight available to melt snow, a factor not accounted for in the model.

Lack of available radiation data necessitated the use of a shortwave radiation model. However, the presence of clouds with high albedo can reflect much of this radiation and affect snowmelt. In addition, the lack of a snowmelt algorithm that is affected by shadowing effect of canopy may cause the rate of snowmelt to be overestimated. Jost *et al*. (2012) mentions that it is necessary to model the spatial variation in melt rates induced by topography and land cover in order to reproduce streamflow. If a model has too much spatial aggregation, this will not be possible.

4 Results and Analysis

4.1 Results

After running the model, the simulated outflow of the catchment was compared with the observed flow data from Bragg Creek station during the study period. The root mean squared error of the simulated flow is about 10.482 cubic metres per second.

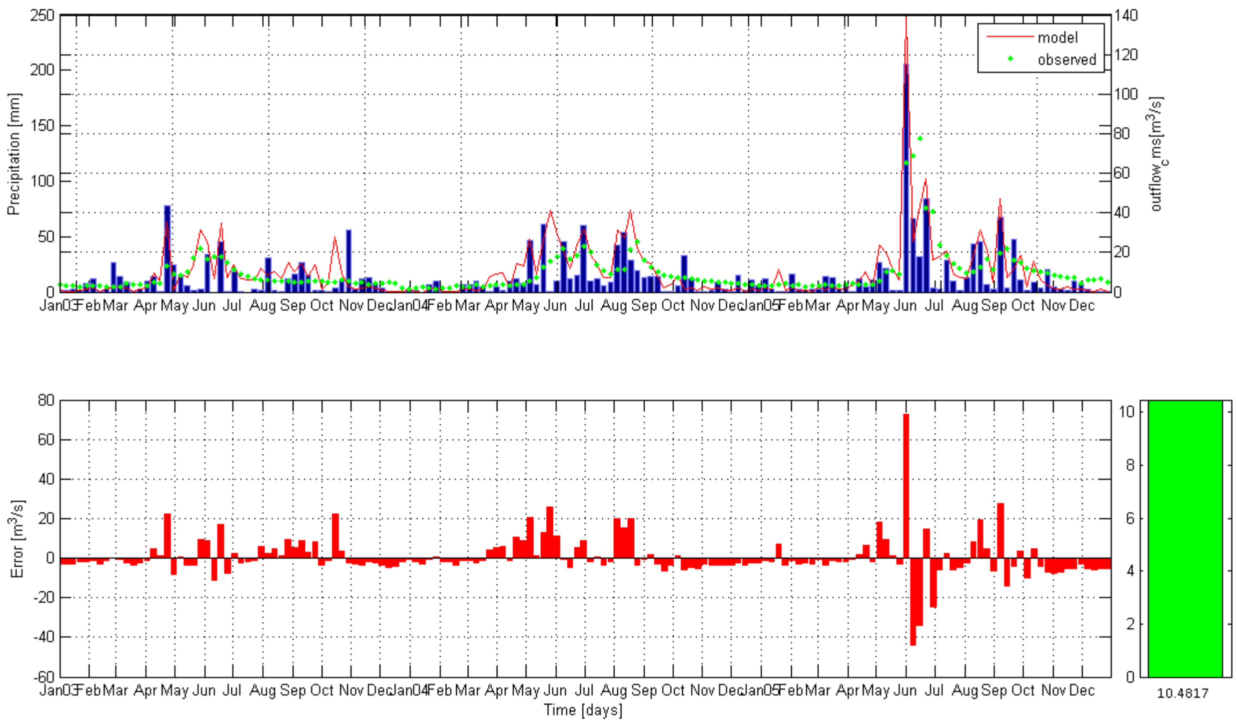

Figure 5: Run results of the model, without an MPB infestation

Scenario conditions simulating beetle attacks of varying degrees were created using the Sims *et al.* MPB model. Initial pest mortality (π_0), beetle fecundity (φ), and curvature parameter (ν) were adjusted for each of the scenarios, and water yield was recorded to observe the effect of beetle infestation. The first values for pest mortality of 0.1560 and 0.7560 to represent low and high infestations, respectively, were taken from Sims *et al.* (2010). Beetle fecundity and curvature were adjusted to determine the model's sensitivity to these parameters. The resulting parameter values for each scenario are shown in Table 4 below:

Table 4: Scenario Parameter Settings

	HRU4: Upper Basin			HRU6: Loam Section			HRU8: ClayLoam Section		
Scenario	π_0	φ	ν	π_0	φ	ν	π_0	φ	ν
BaseCase	0	N/A	N/A	0	N/A	N/A	0	N/A	N/A
LowInf	0.1560	13360	0.2	0.1560	13360	0.2	0.1560	13360	0.2
HighInf	0.7560	13360	0.2	0.7560	13360	0.2	0.7560	13360	0.2
MixedInf	0.7560	13360	0.2	0.1560	13360	0.2	0.1560	13360	0.2
HalfFecund	0.7560	6680	0.2	0.1560	6680	0.2	0.1560	6680	0.2
DblFecund	0.7560	26720	0.2	0.1560	26720	0.2	0.1560	26720	0.2
TplFecund	0.7560	40080	0.2	0.1560	40080	0.2	0.1560	40080	0.2
QplFecund	0.7560	53440	0.2	0.1560	53440	0.2	0.1560	53440	0.2
HalfNu	0.7560	13360	0.1	0.1560	13360	0.1	0.1560	13360	0.1
DblNu	0.7560	13360	0.4	0.1560	13360	0.4	0.1560	13360	0.4
Fecundx100	0.7560	1336000	0.2	0.1560	1336000	0.2	0.1560	1336000	0.2

The resulting simulation runs were recorded with the resulting water yield and RMSE compared to the BaseCase scenario shown below in Table 5:

Table 5: Scenario Results

	Water Yield [m³]			Percentage Difference [%age]				RMSE
Scenario	**2003**	**2004**	**2005**	**2003**	**2004**	**2005**	**Average**	**[m³/s]**
BaseCase	3217.2	4241.7	8321.3	-	-	-	-	-
LowInf	3176.3	4196.4	8364.7	-1.271	-1.068	0.522	-0.606	1.0013
HighInf	3172.2	4195.7	8363.5	-1.399	-1.084	0.507	-0.659	1.0265
MixedInf	3173.9	4196.7	8363.4	-1.346	-1.061	0.506	-0.634	1.0175
HalfFecund	3210.7	4232.3	8324	-0.202	-0.222	0.032	-0.130	0.15634
DblFecund	3065.0	4332.9	8541.7	-4.731	2.150	2.649	0.023	3.1194
TplFecund	3020.2	4456.5	8581.4	-6.123	5.064	3.126	0.689	3.5771
QplFecund	2997.7	4482.1	8573.7	-6.823	5.668	3.033	0.626	3.6844
HalfNu	3209.4	4227.7	8335.4	-0.242	-0.330	0.169	-0.134	0.25446
DblNu	2995.4	4426.5	8506.2	-6.894	4.357	2.222	-0.105	3.3976
Fecundx100	2991.1	4514.6	8574.5	-7.028	6.434	3.043	0.816	3.7796

4.2 Discussion

The largest error occurred during May to June 2005, when high rainfall caused flooding in the watershed. The subsequent weeks also showed the largest underestimation of flow. The largest errors appeared to match periods of significant precipitation, suggesting that the model is inadequate to handle extraordinary precipitation events. 2005 has a higher peak weekly precipitation than the preceding two years by almost 250%, and the model is unable to handle the sudden increase, filling the soil moisture and producing a great deal of outflow, and in the next time step, greatly underestimates the predicted flow. This suggests that the flow concentrates within a time step, and that the storage algorithms for the model are insufficient to accurately simulate actual storage processes. Instead of flow concentrating inside of a time step, the storage of the model should be attenuating this flow and allowing it to release slowly.

The scenarios are intended describe a variety of cases varying the impact of the MPB, comparing it to a base case with no infestation. The largest difference from the base case is found by varying beetle fecundity (φ), but even large increases in fecundity produce a change in flow of only 3.78 m^3/s, which is well below the RMSE of the base case when compared with the observed flow data, suggesting that any impact of MPB would be obscured by discrepancy between the model and observed reality.

MPB infestations reduce forest cover, which serves to reduce canopy moisture storage and synchronize flow, but these effects can also be mimicked with a weekly model time step and a high precipitation year. Therefore, effects of MPB could be obscured because of the study period chosen. Hélie *et al.* (2005) noted that changes in peak flow magnitude and timing in watersheds governed by snowmelt was highly variable, ranging from no effect to 60% higher peaks, and these peaks could be pushed forward anywhere from 0 to 18 days.

Pugh and Gordon (2012) also noted that the previous studies on the effects of bark beetle attacks are based on changes to forest cover, particularly from harvesting. However, harvesting itself may change water yields more than death by beetle infestation. This is because even in the "dead" stands in the gray attack phase, 20 – 30% of the trees are still living, and often the younger immature trees have higher ET rates than the mature trees which are the targets of the beetles' attacks. In addition, mechanical equipment used for harvesting may compact the soil, lowering infiltration rates and increasing soil runoff. These effects may over-represent the increased water yield due to MPB in previous studies.

5 Recommendations

5.1 Conclusion

The Upper Elbow River watershed was modelled using physically based algorithms to determine water flow parameters. The study area was divided into 8 HRUs and separated into two basic categories: rocky terrain and forested terrain, each with appropriate sub modules. The model responded well except for the final year in 2005 where the model could not handle the sudden burst of precipitation.

Although the model was completed, it could not be confirmed that a large-scale MPB infestation would greatly affect the hydrological condition of the watershed, because the change in water yield for each scenario did not exceed the RMSE of the model compared with observed outflow data.

5.2 Recommendations

The models explored in this project should be expanded to take into account the effects of climate to the MPB's spread and development. More sophisticated models would simulate the acceleration of the beetle's development in warmer and wetter conditions, and a threshold factor, above which MPB would spread to neighbouring HRUs. The beetle's preference for trees older than 80 years old (Coggins *et al.*, 2008; Ritchie, 2008) and for particular stand densities could also be further modelled (Safranyik *et al.*, 1999), as the expected distance MPB has been observed to disperse is about 20 m (Safranyik *et al.*, 1992).

Climate and water availability also affect the host's ability to defend against attack – this factor is abstracted as the *a* parameter in the Sims, Aadland and Finnoff MPB model, and further study can be done on the precise nature of the relationship between climate and water availability and this parameter.

A detection factor could be added to simulate the efficacy of various forest management practices. This detection factor would take the beetle's density and the method of control and subsequently reduce the next brood's potential adult populations. With the detection modelling in place, four forest management scenarios can be performed. One scenario is a baseline simulation of the watershed area without a large-scale MPB outbreak. The second scenario will simulate an unchecked MPB outbreak. The third scenario will model the same outbreak, but with current Forest Management policies in place. The fourth scenario will model the same MPB outbreak, but with a different Forest Management policy in place.

Bibliography

Shields, J.A., Tarnocai, C., Valentine, K.W.G., & MacDonald, K.B. (1991). *Soil landscapes of Canada: Procedures manual and user's handbook* (Publication 1868/E), Agriculture Canada, 73 pages.

American Society of Civil Engineers. (2005). *The ASCE standardized reference evapotranspiration equation*. Allen, R.G. *et al*. (Eds.), 70 pages.

Annandale, J.G., Jovanovic, N.Z., Benadé, N., & Allen, R.G. (2002). Software for missing data error analysis of Penman-Monteith reference evapotranspiration. *Irrigation science*, *21*(2), 57-67. doi:10.1007/s002710100047

BC Ministry of Forests and Range (2012). *Provincial-Level Projection of the Current Mountain Pine Beetle Outbreak*. Retrieved Feb 24, 2012 from http://www.for.gov.bc.ca/hre/bcmpb/.

Bewley, D., Alila, Y., & Varhola, A. (2010). Variability of snow water equivalent and snow energetics across a large catchment subject to Mountain Pine Beetle infestation and rapid salvage logging. *Journal of Hydrology*, *388*(3/4), 464-479. doi:10.1016/j.jhydrol.2010.05.03

Bow River Basin Council. (2005). Chapter 6: Reach 4 – Bearspaw Dam to Upstream of the Western Irrigation District Weir. In *BRBC Bow River Report* (pp. 83-106).

Canadian Forestry Service. (1982). *A Review of Mountain Pine Beetle Problems in Canada*, Victoria, BC, 27 pages.

Chang, M.T. (2003). *Forest Hydrology: An Introduction to Water and Forests*. New York, NY: CRC, 373 pages.

Coggins, S.B., Coops, N.C., & Wulder, M.A. (2008). Initialization of an insect infestation spread model using tree structure and spatial characteristics derived from high spatial resolution digital aerial imagery. *Canadian Journal of Remote Sensing*, *34*(6), 485-502.

Coggins, S.B., Coops, N.C., Wulder, M.A., Bater, C.W., & Ortlepp, S.M. (2010). Comparing the impacts of mitigation and non-mitigation on mountain pine beetle populations. *Journal of Environmental Management*, *92*, 112-120. doi:10.1016/j.jenvman.2010.08.016

Dai, Q.F. (2010). *Iterative interpolation of daily precipitation data over Alberta. Library and archives Canada* (Master's thesis). University of Alberta, Edmonton, AB, 194 pages.

Denoth, A. (2003). Structural phase changes of the liquid water component in Alpine snow. *Cold Regions Science and Technology*, *37*, 227-232. doi:10.1016/S0165-232X(03)00066-1

FAO - Food and Agriculture Organization of the United Nations. (1998). Crop evapotranspiration - Guidelines for computing crop water requirements. Retrieved Feb 26, 2012, from http://www.fao.org/docrep/X0490E/X0490E00.htm

Gartner Lee Limited. (2008). *Yukon Soil Database Manual* (GLL70098), Forestry Management Branch, Energy Mines and Resources, Yukon Government, 46 pages.

Gray, D.M., & Landine, P.G. (1987). Albedo model for shallow prairie snow covers. *Canadian Journal of Earth Sciences*, *24*, 1760-1768. doi:10.1139/e87-168

Hayashi, M. (2011). Evaporation. Retrieved from http://people.ucalgary.ca/~hayashi/glgy607/lectures/glgy607f11_ch4.pdf

Hedstrom, N.R., & Pomeroy, J.W. (1998). Measurements and modelling of snow interception in the boreal forest. *Hydrological Processes*, *12*(10/11), 1611-1625.

doi:10.1002/(SICI)1099-1085(199808/09)12:10/11<1611::AID-HYP684>3.0.CO;2-4

Hélie, J.F., Peters, D.L., Tattrie, K.R., & Gibson, J.J. (2005). *Review and Synthesis of Potential Hydrologic Impacts of Mountain Pine Beetle and Related Harvesting Activities in British Columbia* (CFS Catalog ID 25684). Canadian Forest Service, 26 pages.

Jost, G., Moore, R.D., Smith, R., & Gluns, D.R. (2012). Distributed temperature-index snowmelt modelling for forested catchments. *Journal of Hydrology*, *420-421*, 87-101. doi:10.1016/j.jhydrol.2011.11.045

Longley, R.W. (1972). The climate of the prairie provinces (Climatological Studies No. 13), Environment Canada, Atmospheric Environment Service, 79 pages.

Maclauchlan, L. (2009). The mountain pine beetle story: The path of outbreak & future opportunities. *Mountain Pine Beetle & Water Resources Workshop*, Kelowna, BC.

O'Halloran, T.L., Law, B.E., Goulden, M.L., Wang, Z.S., Barr, J.G., Schaaf, C., Brown, M., Fuentes, J.D., Göckede, M., Black, A., & Engel, V. (2011). *Radiative forcing of natural forest disturbances, Global Change Biology*, 1-11.

Pellicciotti, F., Brock, B., Strasser, U., Burlando, P., Funk, M., & Corripio, J. (2005). An enhanced temperature-index glacier melt model including the shortwave radiation balance: development and testing for Haut Glacier d'Arolla, Switzerland. *Journal of Glaciology*, *51*(175), 573-587.

Potts, D.F. (1984). Hydrologic Impacts of a Large-Scale Mountain Pine Beetle (*Dentroctonus ponderosae Hopkins*) Epidemic. *Journal of the American Water Resources Association*, *20*(3), 373-377. doi:10.1111/j.1752-1688.1984.tb04719.x

Pugh, E., & Gordon, E. (2012). A conceptual model of water yield effects from beetle-induced tree death in snow-dominated lodgepole pine forests. *Hydrological Processes*, 13 pages. doi:10.1002/hyp.9312.

Ritchie, C. (2008). Management and Challenges of the Mountain Pine Beetle Infestation in British Columbia. *Alces*, *44*, 127-135.

Safranyik, L., Linton, D.A., Silversides, R., & McMullen, L. (1992). Dispersal of released mountain pine beetles under the canopy of a mature lodgepole pine stand. *Journal of Applied Entomology*, *113*, 441–450.

Safranyik, L., Barclay, H., Thomson, A.G., & Riel, W. (1999). *A population dynamics model for the mountain pine beetle, Dendroctonus ponderosae Hopkins* (Information Report BC-X-386), Pacific Forestry Centre, 35 pages.

Schmidt, R. A., & D. R. Gluns. (1991). Snowfall interception on branches of three conifer species, *Canadian Journal of Forest Research*, *21*, 1262-1269.

Schnorbus, M. (2009). *Quantifying the peak flow impacts of Mountain Pine Beetle and salvage harvest in the Fraser River drainage*. FORREX Mountain Pine Beetle and Water Management Conference Proceedings.

Silva Ecosystem Consultants Ltd. (1993). *Mountain Pine Beetle Literature Review*. Vallican, BC: Bradley, T. 16 pages.

Sims, C., Aadland, D., & Finnoff, D. (2010). A dynamic bioeconomic analysis of Mountain Pine Beetle epidemics. *Journal of Economic Dynamics & Control*, *34*, 2407-2419. doi:10.1016/j.jedc.2010.06.010

Skakun, R.S., Wulder, M.A., & Franklin, S.E. (2003). Sensitivity of the thematic mapper enhanced wetness difference index to detect mountain pine beetle red-attack damage. *Remote Sensing of Environment*, *86*(4), 433-443. doi:10.1016/S0034-4257(03)00112-3

Strasser, U., Warscher, M., & Liston, G.E. (2011). Modeling snow-canopy processes on an idealized mountain. *American Meteorological Society*, *12*(4), 663-677. doi:10.1175/2011JHM1344.1

Sumner, D.M. & Jacobs, J.M. (2005). Utility of Penman-Monteith, Priestley-Taylor, reference evapotranspiration, and pan evaporation methods to estimate pasture evapotranspiration. *Journal of Hydrology*, *308*, 81-104.

Thomson, A.J., & Shrimpton, D.M. (1984). Weather associated with the start of Mountain Pine Beetle outbreaks. *Canadian Journal of Forest Research*, *14*(2), 255-258. doi:10.1139/x84-049

US Army Corps of Engineers (1994). Chapter 5 – Snow Analysis (Report No. EM 1110-2-1418), US Army Corps of Engineers, 12 pages.

US Army Corps of Engineers (2000). HEC-HMS Technical Reference Manual, US Army Corps of Engineers, 157 pages.

Wigmosta, M.S., Vail, L. W., & Lettenmaier, D. P. (1994). A distributed hydrology-vegetation model for complex terrain. *Water Resources Research*, *30*(6), 1665-1679. doi:10.1029/94WR00436

Winkler, R. (2009). *Mountain Pine Beetle and watershed hydrology: An overview*. FORREX Mountain Pine Beetle and Water Management Conference Proceedings.

Winkler, R., Boon, S., Zimonick, B., & Baleshta, K. (2010). Assessing the effects of post-pine beetle forest litter on snow albedo. *Hydrological Processes*, *24*, 803-812. doi:10.1002/hyp.7648

Yan, H., Wang, S.Q., Billesbach, D., Oechel, W., Zhang, J.H., Meyers, T., Martin, T.A., Matamala, R., Baldocchi, D., Bohrer, Dragoni, D., Scott, R. (2012). Global estimation of evapotranspiration using a leaf area index-based surface energy and water balance model. *Remote Sensing of Environment*, *124*, 581-595.